Polymer Bulletin (2020) 77:5681–5696
https://doi.org/10.1007/s00289-019-03039-9

ORIGINAL PAPER

Chitosan/reduced graphene oxide/Pd nanocomposites for co-delivery of 5-fluorouracil and curcumin towards HT-29 colon cancer cells

S. Dhanavel[1,2] · P. Praveena[1] · V. Narayanan[3] · A. Stephen[1]

Received: 24 June 2019 / Revised: 3 November 2019 / Accepted: 27 November 2019 /
Published online: 5 December 2019

Abstract

Biopolymer and carbon allotropes-based templates are receiving attention in the biomedical field due to the non-toxic and biocompatible nature. Noble metal nanoparticles (np's) have attracted increasing interest in biomedical field owing to their unique desirable physical, chemical and biological properties. In the present work, novel anticancer drugs-loaded palladium np's on chitosan/reduced graphene oxide (Gr) was synthesized through simple and cost-effective chemical reduction method. 5-Fluorouracil (5-FU) and curcumin-loaded nanocomposites were prepared individually and in conjugated form. Drug-loaded composites were analysed using various characterizations. The size of the drug-coated nanospheres was measured using HRTEM analysis and the size was estimated to be 4–5 nm. Elemental analysis has been carried out using photoelectron spectroscopy and elemental mapping. The release profile has been analysed via different release kinetics. Pd nanospheres on chitosan/Gr facilitate the sustained release of the drug, thus leading to a reduction in the number of doses administered. The cytotoxicity analysis on human colon cancer cells (HT-29) shows efficacy of the system towards effectively hindering the growth of cells.

Keywords Chitosan/reduced graphene oxide/Pd ternary composite · Palladium nanospheres · Drug delivery · HT-29 cells

✉ A. Stephen
stephen_arum@hotmail.com; stephen@unom.ac.in

[1] Department of Nuclear Physics, University of Madras, Guindy Campus, Chennai 600 025, India

[2] Materials Chemistry and Metal Fuel Cycle Group, Indira Gandhi Centre for Atomic Research, Kalpakkam 603102, India

[3] Department of Inorganic Chemistry, University of Madras, Guindy Campus, Chennai 600 025, India

Introduction

In the past two decades, noble metal nanoparticles have been utilized for the development of new drug delivery and therapeutic methods due to their biocompatibility, high stability and ease of synthesis [1]. Among these, silver and gold nanoparticles-based applications in biomedical field are extensively investigated [2]. Recently, photothermal therapy and drug delivery by utilizing these nanoparticles are receiving much attention among researchers. Zhao et al. reported liposome@AgAu nanocomposite for NIR (near-infrared) responsive drug delivery applications [3]. XinDing et al. reported core–shell Au–Ag nanoparticles for simultaneous bacterial imaging and antibacterial activity [4]. Photothermal treatment on bacteria using Au–Ag–Au nanorods was reported by Hu e al. [5]. Consecutively, palladium is extensively studied in the field of catalysis such as fuel cells and hydrogenation processing of environmental pollutants. Despite their remarkable properties, they have not been fully exploited in the nanomedical field. Cytotoxic effect of green synthesized palladium nanoparticles on *Cervical carcinoma* was studied by Shanthi et al. [6] and also suggested Pd nanoparticles in drug delivery applications. Biocompatibility and antibacterial activity of palladium nanoparticles synthesized using fruit extract of *Couroupita guianensis Aubl* was studied and reported that Pd nanoparticles are compatible with red blood cells [7].

In order to enhance their properties, Pd nanoparticles were dispersed using 2D nanostructures and polymeric materials. Al-Marri et al. [8] reported the fabrication of Pd@graphene for enhanced catalytic applications. Polyaniline/Pt–Pd and polyaniline/Au–Pd nanocomposites were synthesized and reported that PANI-stabilized nanoparticles has improved antibacterial activities [9, 10]. Recently, biological materials have been utilized for the dispersion of Pd nanoparticles. Cochlospermum gossypium, a natural biopolymer-supported palladium nanoparticle, was utilized for the reduction of 4-nitrophenol [11]. Palladium nanoparticles with carboxymethyl cellulose for degradation of azo-dyes have been reported by Li et al. [12]. Chitosan is a biopolymer that possesses a non-toxic and biocompatible nature which makes them favourable to prepare eco-friendly nanocomposites suitable for biomedical and environmental remediation applications. Dhanavel et al. [13, 14] have reported that chitosan-supported palladium nanocomposites show better antibacterial and catalytic performance. In this report, chitosan/Pd/Gr ternary nanocomposites were prepared using simple chemical reduction method and characterized.

To the best of our knowledge, the application of chitosan/Pd/Gr as drug carrier for the cancer treatment has not yet been reported. The prepared composite was utilized for the dual-drug delivery applications. Chitosan/Pd nanocomposites loaded with 5-fluorouracil and curcumin for the single drug delivery and dual-drug delivery towards HT-29 have been reported previously by our group [15]. Here, the prepared composites were analysed with different characterizations and utilized as the carrier for delivering drugs individually and in a conjugated form. The cytotoxic effect on HT-29 cells for single drug-loaded and dual-drug-loaded composites was analysed.

Materials and methods

Materials

Curcumin, 5-fluorouracil with ≥ 99% and dimethyl sulfoxide (DMSO) with 99% purity, palladium(II) acetate with 98% purity, chitosan (low molecular weight and ~ 85% deacetylated) were procured from Sigma-Aldrich. Ultra-pure Tween 80 and sodium tripolyphosphate with 98% purity was obtained from Alfa Aesar. Sodium borohydride with 99% purity was purchased from Merck India. Double-distilled water was used for the synthesis, and solvents used were of analytical grade.

Characterization details

The X-ray diffraction (GE X-ray diffraction system-XRD 3003 TT) measurements were carried out at room temperature with CuKα1 radiation ($\lambda = 1.5406$ Å) for $2\theta = 5°–70°$ at a scan rate of 0.04°/s. The particle size and morphology of samples were analysed using HRTEM analysis by FEI TECNAI G2 model T-30 instrument operating at operating voltage of 250 kV. The surface morphology of the samples was analysed using HITACHI SU-6600 field-emission scanning electron microscopy. Elemental mapping was done using FEI Quanta-250 FEG. Raman-11, Nanophoton Corporation, Japan, with the 514-nm laser wavelength was used to record Raman spectra. Fourier-transform infrared spectra were recorded with Shimadzu FTIR 8300 series system in the range 4000–400 cm^{-1}, and measurements were carried out by dispersing the sample in KBr. XPS measurements are carried out with Omicron nanotechnology, Germany (Gmbh), equipped with mono-chromatic X-ray source (Al Ka radiation). C1*s* peak at 284.5 eV was taken as a reference to exclude the charging effect on the sample. UV–visible spectrophotometer PerkinElmer lambda 650 was used to obtain release profile.

Synthesis of drug-loaded chitosan/Gr/palladium

Initially, Gr was prepared using modified hummers method as our previous reports [13, 14]. Then, chitosan solution was mixed with 3.8 mM 5-FU solution. Then, 1.4 mM TPP solution was added to the above suspension containing the ratio of chitosan to TPP as 2:1 and Tween 80 (0.5% (v/v) was added to the above solution. The pH of the solution was maintained between 4.5 and 4.8. This suspension was stirred and sonicated for 180 min at room temperature to allow the drug molecules adsorb onto the nanoparticles. To this, 5 wt% of graphene oxide nanosheets was added and the suspension was stirred for 180 min. The solution of palladium acetate (0.0329 M) equivalent to 5 wt% of chitosan was added to the graphene oxide-loaded suspension. Herewith, 0.65 M of sodium borohydride solution was added to achieve the reduction of palladium acetate to Pd in the solution. A solution of 5-FU@CS/Gr/Pd thus obtained was centrifuged and freeze-dried. The obtained powder was used for further analysis. About 1.32 mM CUR solution was added to prepare CUR@CS/Gr/Pd nanocomposite. For the preparation of

dual-drug-loaded CS/Gr/Pd, 5-FU and CUR solutions (1:1) were added simultaneously and the same procedure was followed as explained in the 5-FU drug encapsulation. Bare CS/Gr/Pd has been prepared for comparison using the same procedure without the addition of drug solution.

Cell lines and culture conditions

The monolayer cell culture was trypsinized, and DMEM (Dulbecco's Modified Eagle Medium) containing 10% FBS (foetal bovine serum) was used to adjust the cell count to 1.0×10^5 cells/ml. The diluted cell suspension (approximately 10,000 cells/well) was added to each well of a 96-well microtitre plate. The supernatant was flicked off when a partial monolayer was formed. Further, 100 µl of different test sample concentrations prepared in maintenance media was added per well in microtitre plates. The plates were incubated at 37 °C in 5% CO_2 atmosphere for 48 h. The sample solutions in the cells were discarded, and 20 µl of MTT (2 mg/ml) was added to the wells. The plates were incubated for 4 h in 5% CO_2 atmosphere at 37 °C. The supernatant was discarded, and DMSO (50 µl) was added to solubilize the formed formazan. The absorbance was measured at a wavelength of 540 nm, and % of growth inhibition was calculated using the following formula (1),

$$\% \text{ Cell viability} = \left[\text{Mean OD of individual test group/Mean OD of control group}\right] \times 100 \quad (1)$$

Results and discussion

Powder XRD

Figure 1 shows the XRD pattern of graphene (Gr), CS/Gr/Pd, 5-FU@CS/Gr/Pd, CUR@CS/Gr/Pd and 5-FU + CUR@CS/Gr/Pd. In the XRD pattern of Gr, the peak was observed at 2θ value of 25.84°. The broad peak at 39.9° which appeared in CS/Gr/Pd, 5-FU@CS/Gr/Pd, CUR@CS/Gr/Pd and 5-FU + CUR@CS/Gr/Pd, corresponds to (111) plane of the face-centred cubic (fcc) structure of Pd. In 5-FU@CS/Gr/Pd, peaks at 26.6° and 30.7° correspond to (1-32) and (-230) planes of triclinic structure of 5-FU. The peaks of 5-FU and CUR affirming the encapsulation of drug molecules into CS/Gr/Pd were observed in the pattern obtained for 5-FU@CS/Gr/Pd and CUR@CS/Gr/Pd, respectively. The diffraction peaks of 5-FU and CUR corroborate well to the ICDD No. 39-1860 and 09-0816, respectively. The presence of diffraction peaks corresponding to 5-FU and CUR in the dual-drug-loaded system confirms the encapsulation of both the drugs into the carrier.

FTIR analysis

Figure 2 shows the FTIR spectra of (a) CS/Gr/Pd, (b) 5-FU@CS/Gr/Pd, CUR@CS/Gr/Pd and 5-FU + CUR@CS/Gr/Pd nanocomposites. The peak located at

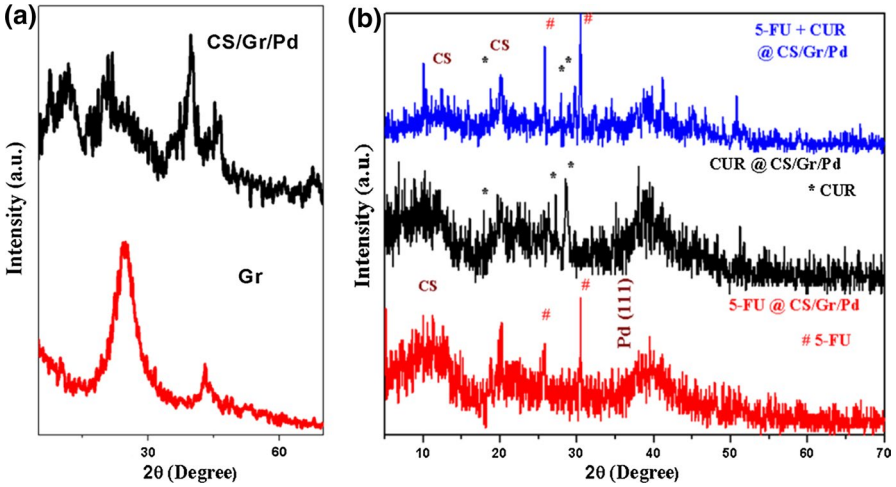

Fig. 1 XRD pattern of **a** Gr and CS/Gr/Pd, **b** drug-loaded CS/Gr/Pd composites

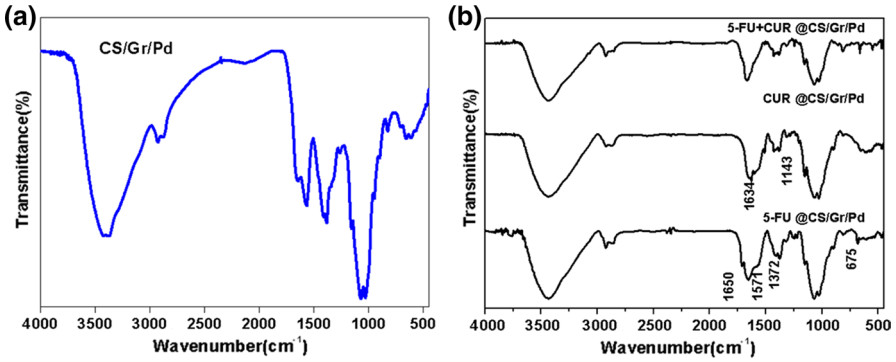

Fig. 2 FTIR spectra of **a** CS/Gr/Pd and **b** drug-loaded CS/Gr/Pd nanocomposites

3464 cm^{-1} corresponds to the stretching band of N–H which overlaps with hydroxyl group. In 5-FU@composite, NH_2 peak was shifted from 1644 to 1650 cm^{-1} and NH_3^+ peak was shifted from 1569 to 1571 cm^{-1} [13, 14, 16]. The peak observed at 675 cm^{-1} is due to the C-H out-of-plane vibration of CF = CH. After CUR is loaded into the composite, a new peak appears at 1143 cm^{-1} when compared to pure nanocomposite [13, 14]. Compared to CS/Gr/Pd, the peak shift is observed at 1634 cm^{-1} which is due to the keto group of curcumin and N–H deformation of chitosan, respectively. The observed shift in the peak of CF = CH and keto group confirms the loading of 5-FU + CUR into the CS/Gr/Pd nanocomposite [13, 14]. In comparison with the 5-FU, CUR and 5-FU + CUR-loaded CS/Pd composites, all the peaks were shifted due to the interaction of Gr with other

moieties [15]. Thus from the study, all the moieties used in the fabrication of composite have been loaded well into the chitosan matrix.

Raman analysis

Figure 3 shows the Raman spectra of (a) CS/Gr/Pd, (b) 5-FU, CUR and 5-FU + CUR-loaded composites. All the samples show two distinct peak at ~ 1360 and ~ 1590 cm^{-1} corresponding to the D band of sp^3 defects of carbon atoms and G band of the graphitic carbon. The I_D/I_G ratio of the 5-FU, CUR and 5-FU + CUR-loaded composites is calculated to be 0.95, 0.86 and 1.15, respectively. While loading drug into the CS/Gr/Pd composite, I_D/I_G ratio has been increased when compared to CS/Gr/Pd. The observed variation is due to the dispersion of Gr nanosheets through the interaction of chitosan, palladium and Gr with the drug molecules. This is confirmed with the observed peak shift compared to the CS/Gr/Pd composites [13, 14].

Electron microscopy (SEM and TEM) analysis

The surface morphology of the drug-loaded composites is given in Fig. 4 which shows the (a) CS/Gr/Pd and (b, c and d) 5-FU + CUR@CS/Gr/Pd nanocomposite with lower and higher magnifications. As compared to the bare nanocomposite [13, 14], Gr in drug-loaded composite exists with surface roughness and distribution of Gr sheets in the composite. This distribution of Gr sheets corroborate well with the obtained Raman spectrum of dual-drug-loaded composite. The appearance of granules (white colour) in the higher magnification images confirms the successful loading of 5-FU and CUR into CS/Gr/Pd nanocomposite. The non-aggregated drug

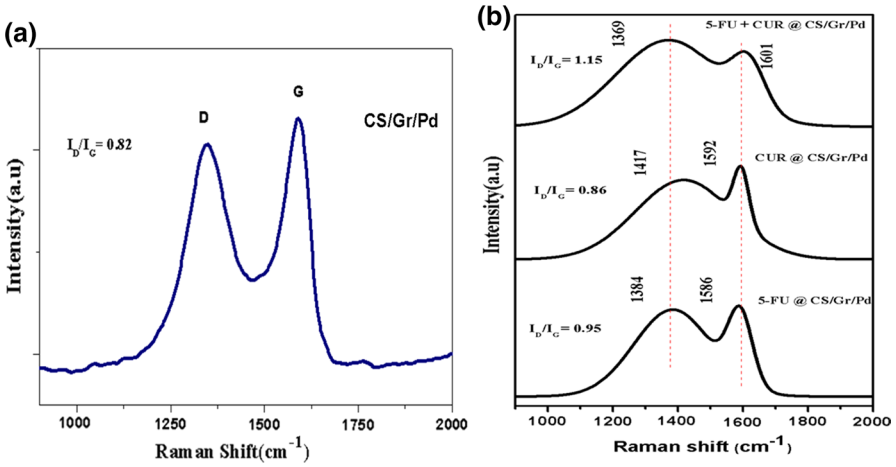

Fig. 3 Raman spectra of **a** CS/Gr/Pd and **b** drug-loaded CS/Gr/Pd nanocomposites

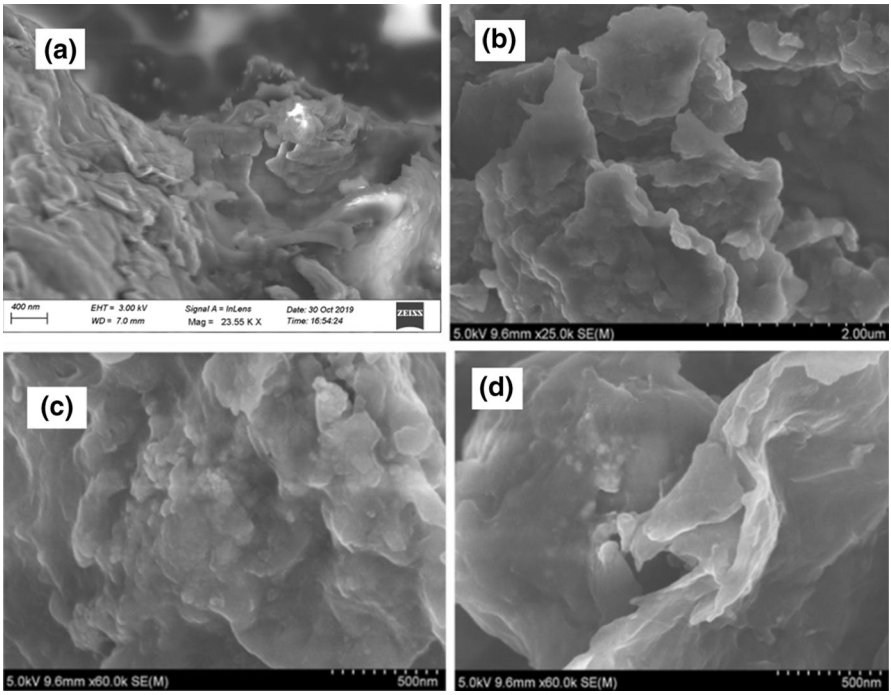

Fig. 4 FESEM images of **a** CS/Gr/Pd and **b**, **c**, **d** dual-drug-loaded CS/Gr/Pd nanocomposites with lower and higher magnifications

loading was achieved due to the π–π interaction and electrostatic interaction between drug molecules and CS/Gr/Pd nanocomposite.

HRTEM images of dual-drug-loaded composites with higher and lower magnifications are shown in Fig. 5a–d. It clearly shows that palladium nanoparticles are spherical in shape, and they are embedded in Gr and chitosan. The particles size was measured using *ImageJ* software, and it was estimated to be 4–6 nm. The particle size of palladium in the drug-loaded composite is on the increase when compared to unloaded composite [13, 14]. The variation is due to the loading of drugs onto the palladium nanoparticles. Particles are aggregated with one another which may be due to binding of curcumin and 5-FU molecules to more than one Pd nanoparticle, thus bringing them close to one another [17]. Further, the interplanar spacing (Fig. 5d) value of palladium has been calculated from the lattice-resolved image and it was found to be as 0.228 nm which matches well to the (111) plane of Pd. The SAED (selected area electron diffraction) pattern of drug-loaded composites is shown in Fig. 5e. The d-spacing values are calculated to be 0.228 nm and 0.142 nm corresponding to (111) and (220) reflections of Pd. The reflection (1–62) corresponding to 5-FU is confirmed from d-spacing value of 0.194 nm. The obtained results concurred well with the XRD results. Based on these higher magnification results, it is concluded that Pd and Gr sheets as filler phase with chitosan as matrix

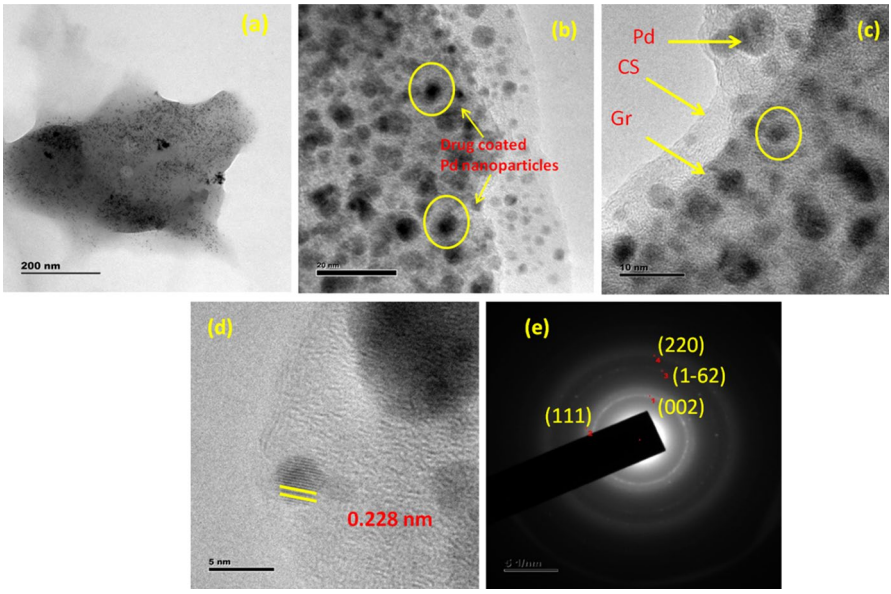

Fig. 5 HRTEM images of **a**–**d** dual-drug-loaded CS/Gr/Pd nanocomposites with lower and higher magnifications and **e** SAED pattern

phase. Thus, the obtained results showed that the formation of composite and drug molecules were entrapped into the composite.

Elemental analysis

Figure 6 shows the X-ray photoelectron spectrum of CS/Gr/Pd nanocomposite. It exhibits the elemental composition of composites containing carbon, palladium, nitrogen and oxygen. It shows that no other impurities are present in the samples. The survey spectrum of CS/Gr/Pd shows shifts when compared to the CS/Pd [15]. It is clear that the addition of Gr plays a vital role in the composites through π–π interaction and electrostatic interaction. The C1*s* spectrum of CS/Gr/Pd consists of three peaks (A, B and C) attributed to C–C (284.7 eV), C–N (286.1 eV) and C–O (287.5 eV), respectively [18–20]. The N1*s* spectra deconvoluted into two peaks at 397.1 eV and 398.8 eV represented as A and B, respectively. The peak A corresponds to NH_2, and B corresponds to NH_3^+, respectively. The existence of NH_3^+ is due to the protonation of amine group of chitosan. The shift of the peaks, NH_2 and NH_3^+ by 2.4 eV and 1.3 eV, respectively, was observed when compared to CS/Pd [15]. It is a well-known fact that NH_2 groups act as a major binding site to the metal nanoparticles where the binding can be attributed to the donation of lone pair of electron from nitrogen to the metal ions, thus leading to the formation of stabilized metal complex. These results affirm the binding of palladium and/or Gr to the NH_2 groups of chitosan. The O1*s* spectrum was deconvoluted into two peaks, namely A

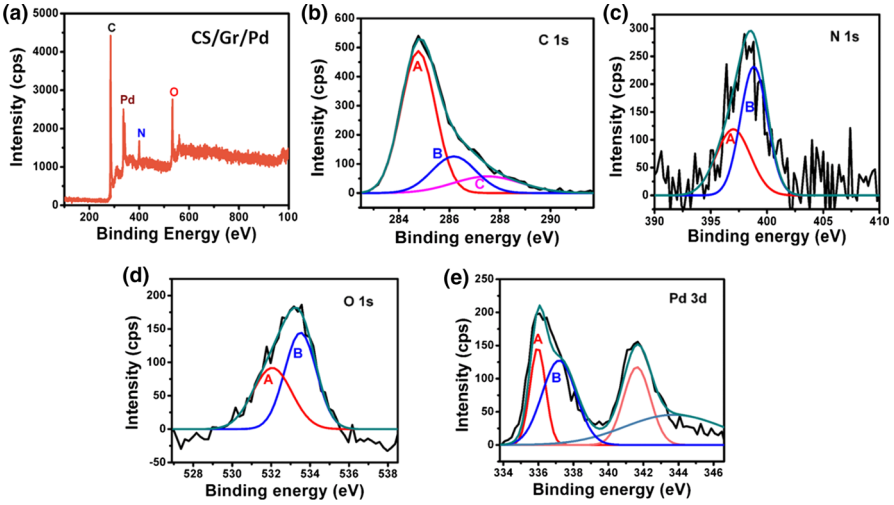

Fig. 6 XPS spectrum of CS/Gr/Pd nanocomposite

and B, as shown in Fig. 6d. The binding energy value of A and B is 531.9 eV and 533.5 eV, corresponding to the C=O and OH, respectively. The atomic concentration of OH was estimated as 61%, whereas in the case of chitosan it is 85% [17]. The variation in the atomic concentration and the peak shift observed when compared to the pure chitosan suggests the interaction of OH groups to the Pd nanoparticles and Gr sheets. The palladium spectrum of CS/Gr/Pd is shown in Fig. 6e. The peaks are deconvoluted into two peaks corresponding to the binding energy of 336.2 eV and 341.4 eV which belongs to metallic palladium (Pd^0). Both the peaks are separated by a binding value of 5.2 eV, and they correspond to $3d_{3/2}$ and $3d_{5/2}$ of Pd^0. The obtained binding energy values shifted from the original binding value of palladium by 0.8 eV [21]. The observed shift to the higher binding energy value is due to the interaction of palladium to the chitosan and Gr [15, 17]. Thus, interaction of palladium and Gr to the NH_2 and OH groups of chitosan is evident from the XPS spectrum.

Elemental mapping of dual-drug-encapsulated nanocomposite with an electron image is given in Fig. 7. It shows mapping of carbon, nitrogen, oxygen, fluorine and palladium. The presence of fluorine in the map confirms the loading of drug into the composite. The interaction of amine group of chitosan to the palladium is evident from nitrogen–palladium electron map and shown in the circle. Similarly, nitrogen and fluorine map confirms the hydrogen bond interaction of amine to the 5-FU molecules as shown in circle.

Determination of drug loading efficiency and encapsulation efficiency

Drug content in the nanoparticles was calculated from the difference between total amount of drug loaded in the carrier and amount of drug untrapped into the carrier.

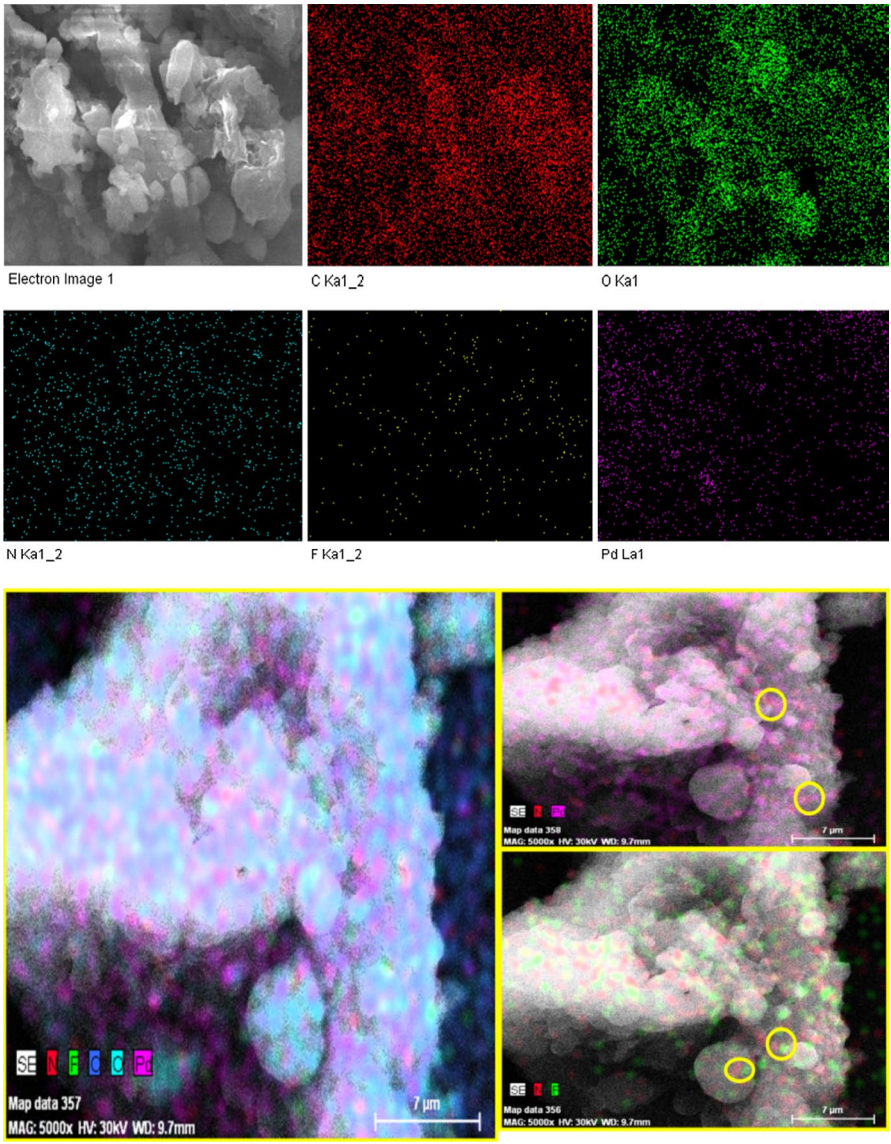

Fig. 7 Elemental mapping of dual-drug-loaded composites

The encapsulation (2) and loading efficiency (3) of the composites were calculated using the formula given as follows.

$$\text{Drug (5-FU or CUR) encapsulation efficiency} = \frac{\text{wt. of } \left[(\text{Total drug}) - (\text{Free drug})\right]}{\text{wt. of total drug}} \times 100\% \quad (2)$$

$$\text{Drug (5-FU or CUR) loading efficiency} = \frac{\text{wt. of } \left[(\text{Total drug}) - (\text{Free drug})\right]}{\text{wt. of drug loaded composite taken}} \times 100\% \quad (3)$$

The isolated supernatant was collected during the centrifugation of the drug-loaded nanocomposites to measure the amount of free drug. An absorbance spectrum of the collected supernatant was taken. The encapsulation and loading efficiencies were calculated (Table 1). The encapsulation efficiency of 5-FU into the 5-FU@CS/Gr/Pd and dual-drug-loaded nanocomposite thus estimated was 98.8% and 95.44%, respectively.

The loading efficiency of the same was estimated to be 25.05% and 18.42%, respectively.

The encapsulation and loading efficiencies of curcumin into the CUR@CS/Gr/Pd system were estimated to be 97.8% and 21.49%, respectively. In the case of dual-drug-loaded system, it was found to be 96.04% and 16.86%. The obtained loading and encapsulation efficiencies are higher than the results obtained for CS/Pd and CS/Gr nanocomposite [15, 16]. The enhanced behaviour is due to the high surface area of palladium nanoparticles and highly dispersed Gr nanosheets giving platform to accommodate the high amount of drug molecules.

Drug release kinetics

CS/Gr/Pd nanocomposites with known amount of drug are suspended in 2 ml phosphate-buffered saline. This suspension was transferred into a dialysis bag (MCWO 1000 Da). The two sides of the bag were sealed and immersed into the 60 ml PBS solution. It was maintained under constant stirring. Three millilitres of the solution was collected from the 60 ml of PBS at regular interval of time, and the amount of drug released was analysed using spectroscopic investigation. The fresh release medium with an equal amount has been replaced into the beaker to maintain constant volume for evaluation.

A calibration graph was plotted for 5-FU and CUR to calculate the amount of drug. Initially, 500 µg of drug (5-FU or CUR) was suspended in phosphate-buffered solution and serial dilution of this solution was used to obtain the remaining concentrations. From the calibration plot, concentration range was taken to fit the absorbance. The cumulative release with respect to time plot for 5-FU, CUR and 5-FU + CUR-loaded systems is shown in Fig. 8.

Table 1 Drug loading efficiency and encapsulation efficiency of drug-loaded CS/Gr/Pd nanocomposites

Sample	Encapsulation efficiency (%)		Drug loading efficiency (%)	
	5-FU	CUR	5-FU	CUR
5-FU@CS/Gr/Pd	98.80	–	25.05	–
CUR@CS/Gr/Pd	–	97.80	–	21.49
5-FU + CUR@CS/Gr/Pd	95.44	96.04	18.42	16.86

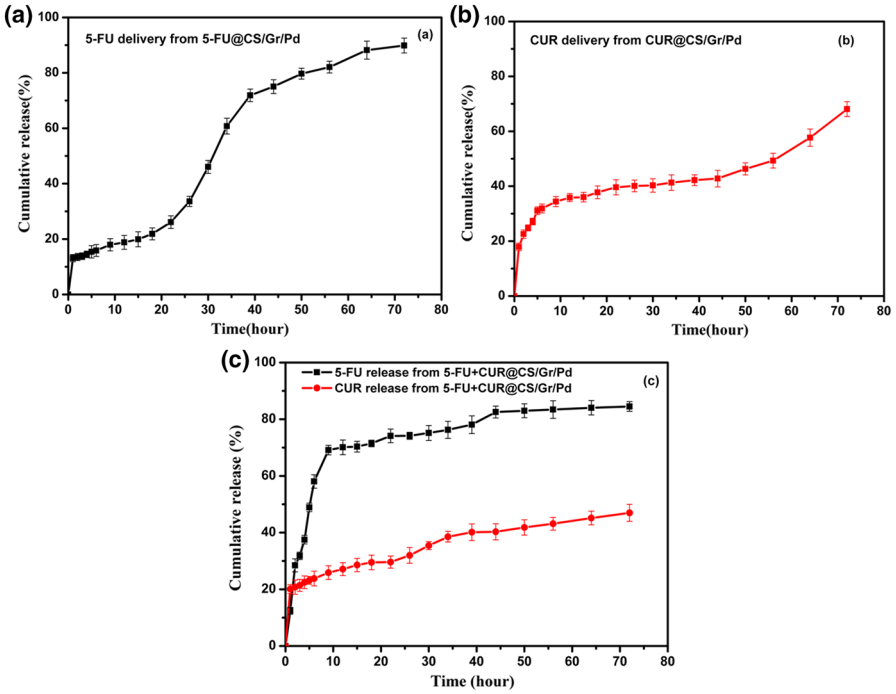

Fig. 8 Drug release profile of **a** 5-FU delivery from the composite **b** CUR delivery from the composite **c** 5-FU and CUR from dual-drug-loaded composite

To analyse the drug release from carrier, different kinetic models were employed to describe the drug release mechanism. Zero-order, first-order, Higuchi, Hixson–Crowell and Korsmeyer–Peppas kinetic models are used to fit the data. The mathematical equations of these kinetic models and their mechanisms are discussed in our previous reports [15, 16]. The kinetic model, which gives the highest correlation coefficient (R^2), is considered as the best fit. The fit between experimental observations and linear function for five kinetic models was done. The R^2 value for the kinetic models fitted on different regions of the release data is given in Table 2.

5-FU release kinetics

According to the highest correlation coefficient, the first region (1–18 h) of the release profile of 5-FU@CS/Gr/Pd fitted well to the Hixson–Crowell kinetics which refers to the drug erosion from CS/Gr/Pd. The second region (22–34 h) matches to the first-order kinetics. The third region (39–72 h) of the release profile shows higher correlation coefficient to Korsmeyer–Peppas model, and the diffusion exponent ($n = 0.37$) of this region suggests that the release follows Fickian diffusion process. While combining with curcumin, the first phase of the 5-FU release in 5-FU + CUR@CS/Gr/Pd adheres to the zero-order kinetics. The adherence of the second (9–39 h) and third regions (44–72 h) were Hixson–Crowell and Higuchi

kinetics, respectively. The best fit of the third model to Higuchi model suggests the diffusion of drug release follows the Fick's law.

CUR release kinetics

The CUR release from CUR@CS/Gr/Pd carrier shows three regions, Region I: 1–6 h, Region II: 9–44 h and Region III: 50–72 h. The first two regions of the release profile adhered well to the Korsmeyer–Peppas kinetic model. The diffusion exponent of these regions was found to be 0.32 and 0.14, respectively, showing the release follows the Fickian diffusion process. The best fit for the third region followed first-order kinetics. In dual-drug-loaded system, the first region (1–18 h) of the release profile fits to the Higuchi model. The second and third regions follow the first-order kinetic model.

Comparison on combined and single delivery

Compared to the chitosan/Pd nanocarrier, initial burst release was reduced in all the delivery systems which is necessary for the effective treatment of cancer [15]. It is due to the π–π interaction and electrostatic interaction of Gr nanosheets playing a vital role in the dispersion of drug into the nanocarrier. About 80% of the 5-FU release was achieved, whereas in the case of CUR, < 70% was observed within 72 h which is due to the hydrophobicity of the drug molecules. In the case of CUR, most of the region adheres to the Korsmeyer–Peppas model in CUR@CS/Gr/Pd, whereas in the case of combined system, most of the region follows the first-order model. It has been already reported that the variation in the kinetics of the drug release

Table 2 Kinetic models' correlation coefficients for drug-encapsulated nanocomposites

Kinetics	Region	5-FU@CS/Gr/Pd	CUR@CS/Gr/Pd	5-FU + CUR@CS/Gr/Pd	
				5-FU@co-delivery	CUR@co-delivery
Zero order	I	01–18 h = 0.9874	01–06 h = 0.9657	01–06 h = 0.9607	01–18 h = 0.9772
	II	22–34 h = 0.9708	09–44 h = 0.9362	09–39 h = 0.9720	22–34 h = 0.9916
	III	39–72 h = 0.9724	50–72 h = 0.9610	44–72 h = 0.9954	39–72 h = 0.9816
First order	I	01–18 h = 0.9748	01–06 h = 0.9338	01–06 h = 0.8482	01–18 h = 0.9597
	II	22–34 h = 0.9975	09–44 h = 0.9229	09–39 h = 0.9706	22–34 h = 0.9956
	III	39–72 h = 0.9655	50–72 h = 0.9787	44–72 h = 0.9950	39–72 h = 0.9838
Korsmeyer–Peppas	I	01–18 h = 0.9008	01–06 h = 0.9850	01–06 h = 0.9556	01–18 h = 0.9418
	II	22–34 h = 0.9870	09–44 h = 0.9773	09–39 h = 0.9415	22–34 h = 0.9847
	III	39–72 h = 0.9850	50–72 h = 0.9574	44–72 h = 0.9969	39–72 h = 0.9585
Hixson–Crowell	I	01–18 h = 0.9884	01–06 h = 0.9698	01–06 h = 0.9593	01–18 h = 0.9804
	II	22–34 h = 0.9443	09–44 h = 0.9414	09–39 h = 0.9731	22–34 h = 0.9895
	III	39–72 h = 0.9811	50–72 h = 0.9401	44–72 h = 0.9964	39–72 h = 0.9800
Higuchi	I	01–18 h = 0.9717	01–06 h = 0.9833	01–06 h = 0.9542	01–18 h = 0.9928
	II	22–34 h = 0.9560	09–44 h = 0.9695	09–39 h = 0.9660	22–34 h = 0.9843
	III	39–72 h = 0.9814	50–72 h = 0.9478	44–72 h = 0.9978	39–72 h = 0.9693

mechanism is due to the combined effect of erosion, pore diffusion in the conjugates, swelling and its degradability [15, 22].

In vitro cytotoxicity analysis

The IC_{50} values, i.e. the concentration of test samples needed to inhibit the growth by 50%, were calculated from the dose-dependent effect on each cell line. Figure 9 shows the cytotoxicity of 5-FU@CS/Gr/Pd, CUR@CS/Gr/Pd and 5-FU + CUR@CS/Gr/Pd.

The cytotoxic effect of all the nanoconjugates against HT-29, human colon carcinoma cell lines with different concentrations, is analysed. Dose-dependent activity was observed for 5-FU@CS/Gr/Pd, CUR@CS/Gr/Pd and 5-FU + CUR@CS/Gr/Pd nanocomposites.

The half-maximal inhibitory concentration, IC_{50} of the 5-FU@CS/Gr/Pd, CUR@CS/Gr/Pd and 5-FU + CUR@CS/Gr/Pd composites, is found to be 13.5 µg/ml, 16.19 µg/ml and 9.87 µg/ml, respectively. It is observed that IC_{50} value of the dual-drug-loaded composite is lesser than that of single drug-loaded composites. The better cell growth inhibition was observed for all the composites when compared to the single/dual-drug-loaded CS/Pd and CS/Gr nanocomposites [15, 16]. The enhanced activity is due to the combined effect of palladium nanoparticles and Gr nanosheets. Moreover, the particle size of palladium reduced in the composite facilitates the anticancer activity when compared to the drug-conjugated CS/Pd composites [16]. The interaction between Gr and Pd with the drug molecules reduces the initial burst release, and this may be the reason for the observed superior activity. The obtained results are comparable with the previous results [2, 16, 17, 23, 24].

Conclusion

Dual-drug-coated palladium nanospheres on chitosan/Gr matrix were successfully synthesized by simple and cost-effective chemical reduction method. XRD analysis was used for structural investigation. The incorporation of drug into the

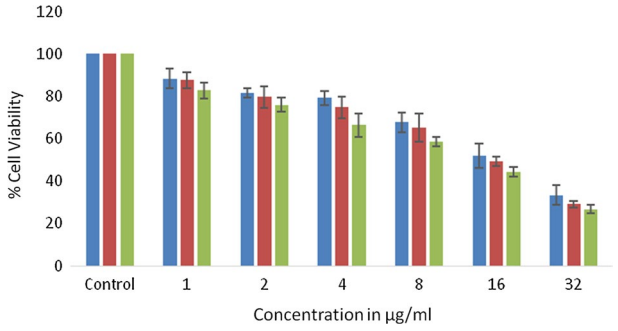

Fig. 9 Cytotoxicity analysis of 5-FU@ CS/Gr/Pd (red), CUR@CS/Gr/Pd (blue) and 5-FU + CUR@CS/Gr/Pd (green) nanocomposites against HT-29 cells

composites is evident from XRD, FTIR and Raman spectroscopy. XPS was used to analyse the presence of elements and chemical environment in the composite. HRTEM results revealed that the palladium nanoparticles are coated by drug molecules, and the results corroborate well with the XRD. Further, it confirms smaller particle size of palladium with approximate diameter of 4–5 nm. The entrapment and loading efficiencies of drugs from 5-FU + CUR@CS/Gr/Pd were estimated to be 95.44% and 18.42% for 5-FU and 96.04% and 16.86% for CUR, respectively. The drug release profile was analysed using five different mathematical models. The cytotoxicity study towards human colon carcinoma cell lines was carried out. The half-maximal inhibitory concentration of the 5-FU@CS/Gr/Pd, CUR@CS/Gr/Pd and 5-FU + CUR@CS/Gr/Pd composites is determined to be 13.5 µg/ml, 16.19 µg/ml and 9.87 µg/ml, respectively. Synergistic activity of drug-loaded CS/Gr/Pd was compared with CS/Pd and CS/Gr.

Acknowledgement One of the authors, S. Dhanavel would like to thank UGC-UPE (Phase II) for providing fellowship to complete this work successfully. SAIF, IIT Madras, is acknowledged for FTIR and Raman measurements. Authors would like to thank Mr. Viswanathan, Vellore Institute of Technology, and Mr. K.C. Dharani balaji IIT Madras, for HRTEM and elemental mapping measurements.

Compliance with ethical standards

Conflict of interest Authors declare no conflict of interest.

References

1. Klębowski B, Depciuch J, Parlińska-Wojtan M, Baran J (2018) Applications of noble metal-based nanoparticles in medicine. Int J Mol Sci 19(12):4031
2. Nivethaa EAK, Dhanavel S, Narayanan V, Stephen A (2017) Chitosan stabilized Ag–Au nanoalloy for colorimetric sensing and 5-fluorouracil delivery. Int J Biol Macromol 95:862–872
3. Zhao Y, Zhao J, Shan G, Yan D, Chen Y, Liu Y (2017) SERS-active liposome@Ag/Au nanocomposite for NIR light-driven drug release. Colloids Surf B 154:150–159
4. Ding X, Yuan P, Gao N, Zhu H, Yang YY, Xu QH (2017) Au–Ag core-shell nanoparticles for simultaneous bacterial imaging and synergistic antibacterial activity. Nanomed Nanotechnol Biol Med 13(1):297–305
5. Hu B, Wang N, Han L, Chen M-L, Wang J-H (2015) Core–shell–shell nanorods for controlled release of silver that can serve as a nanoheater for photothermal treatment on bacteria. Acta Biomater 11:511–519
6. Shanthi K, Sreevani V, Vimala K, Kannan S (2017) Cytotoxic effect of palladium nanoparticles synthesized from syzygium aromaticum aqueous extracts and induction of apoptosis in *Cervical carcinoma*. Proc Natl Acad Sci India Sect B Biol Sci 87(4):1101–1112
7. Gnanasekar S, Murugaraj J, Dhivyabharathi B, Krishnamoorthy V, Jha KP, Seetharaman P, Sivaperumal S (2018) Antibacterial and cytotoxicity effects of biogenic palladium nanoparticles synthesized using fruit extract of *Couroupita guianensis* Aubl. J Appl Biomed 16(1):59–65
8. Al-Marri AH, Khan M, Shaik MR, Mohri N, Adil SF, Kuniyil M, Siddiqui MRH (2016) Green synthesis of Pd@graphene nanocomposite: catalyst for the selective oxidation of alcohols. Arab J Chem 9(6):835–845
9. Boomi P, Prabu HG (2013) Synthesis, characterization and antibacterial analysis of polyaniline/Au–Pd nanocomposite. Colloids Surf A 429:51–59
10. Boomi P, Prabu HG, Mathiyarasu J (2014) Synthesis, characterization and antibacterial activity of polyaniline/Pt–Pd nanocomposite. Eur J Med Chem 72:18–25

11. Rastogi L, Beedu SR, Kora AJ (2015) Facile synthesis of palladium nanocatalyst using gum kondagogu (*Cochlospermum gossypium*): a natural biopolymer. IET Nanobiotechnol 9(6):362–367
12. Li G, Li Y, Wang Z, Liu H (2017) Green synthesis of palladium nanoparticles with carboxymethyl cellulose for degradation of azo-dyes. Mater Chem Phys 187:133–140
13. Dhanavel S, Manivannan N, Mathivanan N, Gupta VK, Narayanan V, Stephen A (2018) Preparation and characterization of cross-linked chitosan/palladium nanocomposites for catalytic and antibacterial activity. J Mol Liq 257:32–41
14. Dhanavel S, Revathy TA, Padmanaban A, Narayanan V, Stephen A (2018) Highly efficient catalytic reduction and electrochemical sensing of hazardous 4-nitrophenol using chitosan/rGO/palladium nanocomposite. J Mater Sci Mater Electron 29(16):14093–14104
15. Dhanavel S, Nivethaa EAK, Narayanan V, Stephen A (2017) In vitro cytotoxicity study of dual drug loaded chitosan/palladium nanocomposite towards HT-29 cancer cells. Mater Sci Eng C 75:1399–1410
16. Dhanavel S, Revathy TA, Sivaranjani T, Sivakumar K, Palani P, Narayanan V, Stephen A (2019) 5-Fluorouracil and curcumin co-encapsulated chitosan/reduced graphene oxide nanocomposites against human colon cancer cell lines. Polym Bull
17. Nivethaa EAK, Dhanavel S, Narayanan V, Vasu CA, Stephen A (2015) An in vitro cytotoxicity study of 5-fluorouracil encapsulated chitosan/gold nanocomposites towards MCF-7 cells. RSC Adv 5(2):1024–1032
18. Buzzacchera I, Vorobii M, Kostina NY, de los Santos Pereira A, Riedel T, Bruns M, Rodriguez-Emmenegger C (2017) Polymer brush-functionalized chitosan hydrogels as antifouling implant coatings. Biomacromol 18(6):1983–1992
19. Dhanavel S, Nivethaa EAK, Dhanapal K, Gupta VK, Narayanan V, Stephen A (2016) α-MoO_3/polyaniline composite for effective scavenging of Rhodamine B, Congo red and textile dye effluent. RSC Adv 6(34):28871–28886
20. Yang J, Duan J, Zhang L, Lindman B, Edlund H, Norgren M (2016) Spherical nanocomposite particles prepared from mixed cellulose–chitosan solutions. Cellulose 23(5):3105–3115
21. Yang X, Li Q, Wang H, Huang J, Lin L, Wang W, Jia L (2010) Green synthesis of palladium nanoparticles using broth of *Cinnamomum camphora* leaf. J Nanopart Res 12(5):1589–1598
22. Xiao B, Si X, Han MK, Viennois E, Zhang M, Merlin D (2015) Co-delivery of camptothecin and curcumin by cationic polymeric nanoparticles for synergistic colon cancer combination chemotherapy. J Mater Chem B 3(39):7724–7733
23. Nivethaa EAK, Dhanavel S, Narayanan V, Stephen A (2016) Fabrication of chitosan/MWCNT nanocomposite as a carrier for 5-fluorouracil and a study of the cytotoxicity of 5-fluorouracil encapsulated nanocomposite towards MCF-7. Polym Bull 73(11):3221–3236
24. Nivethaa EAK, Dhanavel S, Rebekah A, Narayanan V, Stephen A (2016) A comparative study of 5-fluorouracil release from chitosan/silver and chitosan/silver/MWCNT nanocomposites and their cytotoxicity towards MCF-7. Mater Sci Eng C 66:244–250